J Solid State Electrochem (2011) 15:421–430
DOI 10.1007/s10008-010-1091-z

ORIGINAL PAPER

Influence of acidic ionic liquids as an electrolyte additive on the electrochemical and corrosion behaviors of lead-acid battery

Behzad Rezaei · Elaheh Havakeshian · Abdol R. Hajipour

Received: 11 January 2010 / Revised: 25 April 2010 / Accepted: 28 April 2010 / Published online: 25 May 2010

Abstract The aim of this study is to introduce the application of some acidic ionic liquids (ILs) as an electrolyte additive in lead-acid batteries. A family of alkylammonium hydrogen sulfate ILs, which are different in the number of alkyl chain, is investigated with the aim to compare their effects on the electrochemical behavior of Pb–Sb–Sn alloy in sulfuric acid solution. The hydrogen and oxygen gas evolution potential and anodic layer characteristics were investigated employing cyclic and linear sweep voltammetric methods. The morphological changes of the $PbSO_4$ layer that formed on the electrode surface were confirmed using scanning electron microscopy. Also, potentiodynamic polarization curves, electrochemical impedance spectroscopy, and an equivalent circuit analysis were used to evaluate the corrosion behaviors of the Pb–Sb–Sn alloy in the presence of ILs. The obtained results indicate that hydrogen and oxygen evolution overpotential of lead–antimony–tin alloy increases in the solution containing IL and mainly depends on the number of alkyl chain in alkylammonium cation. It is clearly observed that the morphology of $PbSO_4$ layer changes under the influence of ILs. The corrosion studies show an increase in corrosion resistance of lead alloy in the presence of some ILs. Also, the electrochemical effects of ILs in conversion of $PbSO_4$ to PbO_2 and vice versa were investigated by carbon-PbO paste electrode. Cyclic voltammogram of carbon-PbO electrode shows that in the presence of ILs, oxidation and reduction peak currents increase, while reversibility decreases.

Keywords Lead-acid battery · Ionic liquids · Electrolyte additives · Lead–antimony alloy · Grid corrosion · Butylammonium hydrogen sulfate

B. Rezaei (✉) · E. Havakeshian · A. R. Hajipour
Department of Chemistry, Isfahan University of Technology, Isfahan 84156-83111 I.R., Iran
e-mail: rezaei@cc.iut.ac.ir

Introduction

The lead-acid battery is an electrochemical device for storing chemical energy until it is released as electrical energy. It is used extensively as automotive, stationary, and traction batteries throughout the world [1]. Lead-acid batteries offer a number of advantages including low cost of manufacture, rechargeability, easy construction, and good specific power when compared to other advanced batteries [2–4].

It is well known that the properties of battery grids are highly dependent on alloying content. The grids of lead-acid batteries were usually made of lead–antimony alloys containing 3 to 11 wt.% antimony. The necessary mechanical strength and castability are easily achieved with this content of antimony [5]. However, antimony decreases overpotential of hydrogen evolution at the negative plate, which leads to early decomposition of water, increase of the self-discharge for batteries, and further, the premature loss of the battery capacity [6, 7]. An attempt was made to decrease the antimony content in the alloys. However, the absence of antimony in the positive electrode of the battery leads to a decrease in its capacity during cycling, or the charging and discharging processes of the lead-acid battery [8]. Various metals have been added to replace antimony such as calcium, tin, arsenic, and selenium [9, 10]. By replacing the antimonial grid material with lead–calcium alloys, the hydrogen overvoltage of the negative electrode was increased. However, new problems arise because the beneficial effect of antimony on the cycle life of the cell was lost [11]. The use of additives in the electrolyte is another approach that increases the hydrogen and oxygen overpotential and decreases the corrosion rate (CR) of lead alloys and offers improvement of the battery as mentioned in the literature [12–15]. The major problem lies with selecting a suitable additive that is chemically, thermally,

and electrochemically stable in highly corrosive environment [13]. Effects of some electrolyte additives on the electrochemical performance of the lead-acid batteries have been investigated [16–19].

Recently, ionic liquids (ILs), consisting of only cations and anions, have received much attention [20–25]. They provide excellent properties such as high ionic conductivity, low volatility, thermal stabilities, wide electrochemical windows, and environmental friendliness [26]. Ionic liquids are typically organic salts containing nitrogen or phosphorus-based organic cations like quaternary ammonium, alkylpyridinium, alkylpyrrolidinium, alkylphosphonium, and alkylimidazolium, combined with a variety of large anions [27]. Because the unique combination of cations and anions influences the various properties of ILs, they have been described as designer solvents [28]. Nowadays, ILs are being considered as novel liquid electrolytes for electrochemical storage devices such as solar cells [23], fuel cells [24], high-energy density batteries [25, 26], and super capacitors [27].

Hence, in this work, we have studied the electrochemical behaviors of lead–antimony alloy in sulfuric acid solution in the presence of some ILs. All employing ILs were the ammonium hydrogen sulfate derivatives with different alkyl chain and the same anion. Therefore, it can be established how the changes in the structure of cation within family affect hydrogen and oxygen evolution potential and electrochemical properties of lead-acid batteries. Butylammonium hydrogen sulfate (BAHS), isopentyl ammonium hydrogen sulfate (IPAHS), and tri-BAHS were used in this article (Scheme 1). Di-BAHS and tetra-BAHS were studied in our previous articles [29, 30].

Experimental

Apparatus

All voltammetric experiments were performed using SAMA 500 Electroanalyzer System (Isfahan, Iran) connected to a personal computer. Electrochemical impedance spectroscopy (EIS) measurements were performed by employing an Autolab PGSTAT 12, and obtained results were fitted and analyzed using the FRA 4.9 software. For all experiments, a conventional three-electrode system was used, which consisted of a working electrode (Pb–Sb–Sn alloy or carbon–lead oxide paste electrode), a platinum counter electrode, and a saturated calomel electrode (SCE) as the reference electrode.

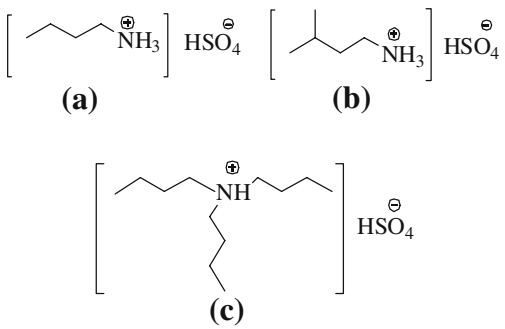

Scheme 1 Molecular structure of **a** BAHS, **b** IPAHS, **c** tri-BAHS

Materials and reagents

Analytical reagent grade chemicals and doubly distilled water were used in preparation of all solutions. Graphite powder and lead oxide powder from Merck (Darmstadt, Germany) and high-viscosity paraffin oil from Fluka (Taufkirchen, Germany) were used for preparation of lead oxide–carbon paste electrode. The electrolyte was 4.0 M sulfuric acid, which was prepared from concentrated H_2SO_4 (Merck) and doubly distilled water. All ILs employed in this study were synthesized and purified in our pharmaceutical research laboratory and were added to 4.0 M sulfuric acid at concentrations 2.5, 5.0, 10.0, 15.0, and 20.0 mg cm^{-3}.

Preparation of working electrodes

The iron mold with cooling system and temperature control unit the same as the grid casting machine of Sovema Co. (Verona, Italy) was used for preparing the working electrode. The working electrode was a wire with geometric area of 0.5 cm^2 around, which was mounted with an epoxy resin. The composition of the alloys was Pb–Sb–0.24 wt.% Sn, in which the content of the antimony was 0.32, 0.50, 0.73, 1.66, 1.88, 2.50, and 2.80 wt.%.

The carbon–lead oxide paste electrode was prepared via mixing 0.1 g of graphite with 0.1 g of lead oxide powder, washed with diethyl ether and dried under vacuum, and then mixed with appropriate amount of mineral oil in a mortar and pestle. The paste was packed into an electrode body, consisting of a plastic cylindrical tube (o.d. 6 mm, i.d. 4 mm), equipped with a copper wire serving as an external electric contact. Before every measurement, the fresh surfaces were obtained by polishing the electrode with a clean paper.

Procedure

In this study, most experiments were carried out using Pb–1.66% Sb–Sn alloy, because in maintenance free batteries, the grids are made with low antimony alloy (1–2 wt.%). Prior to each experiment, the lead alloy electrode was mechanically polished with water-resistant emery paper (P 1000), washed in acetone, and thoroughly rinsed with doubly distilled water to remove oxides and sulfates

formed on the surface of electrode. Cyclic voltammograms (CVs) of lead alloy electrodes in the sulfuric acid solutions with and without IL in the potential region between hydrogen and oxygen evolution (−2.5 to +2.5 V vs. SCE) were obtained at a sweep rate of 50.0 mV s^{-1}.

Micrographs of lead alloy electrodes after one cycle of charge and discharge were obtained with Philips-XL30 (Eindhoven, Netherlands) scanning electron microscope. Before taking scanning electron microscopy (SEM) imaging, a thin layer of gold was deposited on the electrode because epoxy resin is electrically insulator.

For evaluation of the effects of these ILs on the CR of the alloy, linear sweep voltammetry (LSV) and Tafel polarization measurement were carried out with a scan rate of 0.2 mV s^{-1} from −0.2 to +0.2 V related to open-circuit potential. This mentioned potentiodynamic range is corresponding to −0.8 and −0.4 V vs. SCE. Electrochemical impedance spectroscopy measurements were carried out after 40 min of exposure of the lead alloy in the solution to reach a steady-state condition. The frequency range was set from 10^5 to 10^{-1} Hz with potential amplitude of 5.0 mV in open-circuit potential.

The CVs of carbon–lead oxide paste electrode were obtained at the sweep rate 50.0 mV s^{-1}, in the potential range of −0.2 to 1.0 V vs. SCE. All experiments were carried out at room temperature (298 K).

Results and discussion

The electrochemical behaviors of Pb–Sb alloy electrodes and redox reactions that are occurring in acidic solutions are complex and depend on many variables, such as kind and concentration of electrolytes and sweep rate [31, 32]. In this article, particular attention was paid to passive layer characteristics, hydrogen and oxygen evolution potential, Sb dissolution, and corrosion resistance of Pb–Sb alloy electrode in 4.0 M sulfuric acid and IL solutions.

Study of passive layer characteristics formed on lead electrode surface

To study the effect of ILs on the $PbSO_4$ layer characteristics formed on the lead electrode surface, we obtained the CVs of a lead–1.66% antimony electrode in 4.0 M sulfuric acid solutions with and without ILs in a potential range limited by the hydrogen (peak H) and oxygen (peak O) gas evolution (Fig. 1). In the anodic potential sweep of the voltammogram, current peak A_1, corresponding to the oxidation of lead to lead sulfate, was recorded. The transition of PbO_2 to $PbSO_4$ (C_1) and PbO to Pb (C_3) occurs during the cathodic potential sweep [6, 31]. Current peaks C_4 and C_5 were assigned to the reduction of small and large $PbSO_4$ crystals, respectively [33, 34]. The oxidation current peak A_2 and the reduction current peak C_2 are related to the oxidation and reduction of antimony and its species, respectively [6, 43].

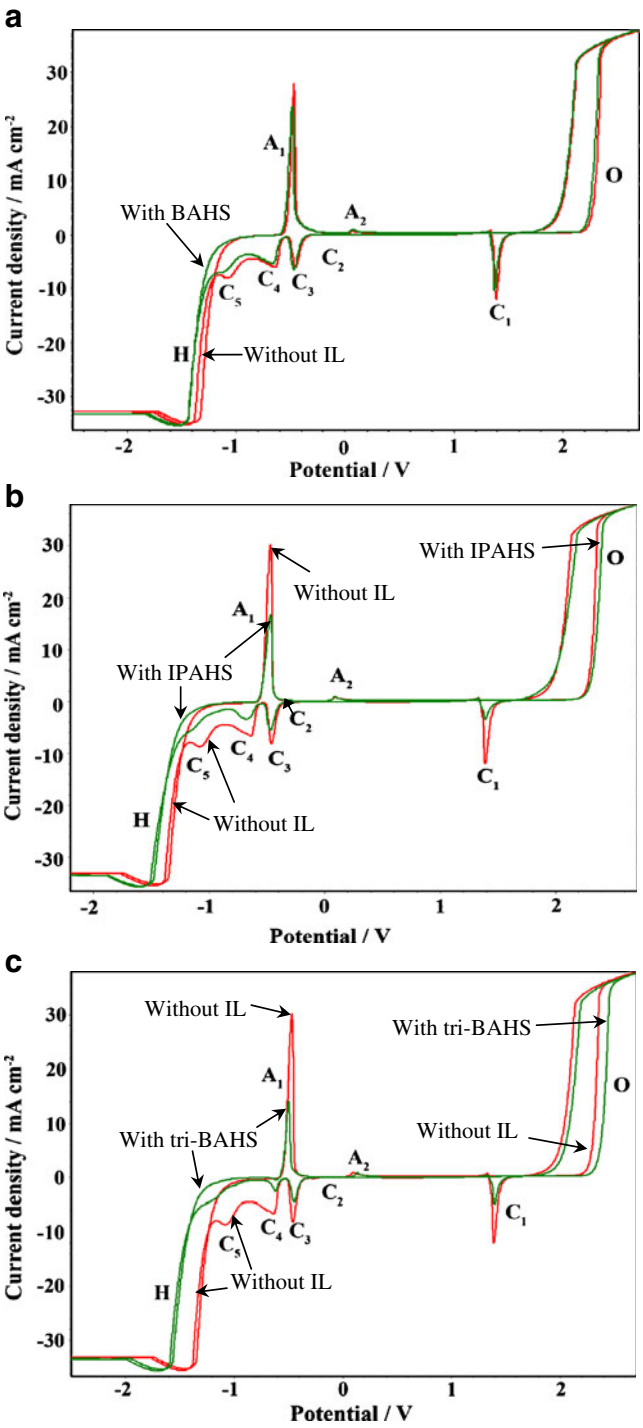

Fig. 1 Cyclic voltammograms of Pb–1.66% Sb–Sn alloy electrode in 4.0 M sulfuric acid solutions with and without 15.0 mg cm^{-3} of IL at sweep rate 50.0 mV s^{-1}. Ionic liquids are **a** BAHS, **b** IPAHS, **c** tri-BAHS

As indicated from peak current A_1 in Fig. 1, in the presence of all studied ILs, the fewer amounts of $PbSO_4$ were formed on the electrode surface, and consequently, the height of the reduction peaks of $PbSO_4$ (peak C_4 and C_5) was diminished. The decrease of current peak C_5, which is related to reduction of large $PbSO_4$ crystals, reveals that formed $PbSO_4$ crystals on the electrode surface in the presence of these ILs are smaller in size. Therefore, the surface morphology of the lead alloy after one cycle of charge and discharge in sulfuric acid solution in the absence and presence of IPAHS and tri-BAHS was obtained to study $PbSO_4$ layer morphology (Fig. 2). The SEM images confirm that smaller and fewer amounts of $PbSO_4$ are formed on the electrode in the presence of IPAHS and tri-BAHS. It seems that cationic species interact with electrode surface and charged species in the electrolyte and, hence, change the structures of basic lead sulfate formed on the electrode surface. It seems that these cations make it difficult for lead and sulfate ions to form lead sulfate crystals and, subsequently, prevent from the growth of existing lead sulfate crystals.

In a comparison between SEM images of IPAHS (Fig. 2b), tri-BAHS (Fig. 2c), and tetra-BAHS [29], it is found that in the solution containing tri-BAHS, smaller lead sulfate crystals have been formed on the electrode surface. Also, the current peak A_1 in Fig. 1, which is related to the forming of $PbSO_4$, has decreased more in the solution containing tri-BAHS than other solutions (Fig. 3a). Therefore, it points out that the amount of interaction between ILs cation and surface electrode and, consequently, the size and amount of lead sulfate crystals mainly depend on the number of butyl chain in alkylammonium cation.

Also, in the passive layer, lead monoxide is formed on lead surface, underneath the $PbSO_4$ membrane [44, 45]. A decrease in the height of current peak C_3 that is related to transition of PbO to Pb demonstrates that lower PbO has been formed underneath the lead sulfate membrane in the presence of all added ILs. Indeed, a decrease in the amount of formed $PbSO_4$ on the electrode surface prevents from increasing pH underneath the lead sulfate membrane, and consequently, fewer PbO is formed.

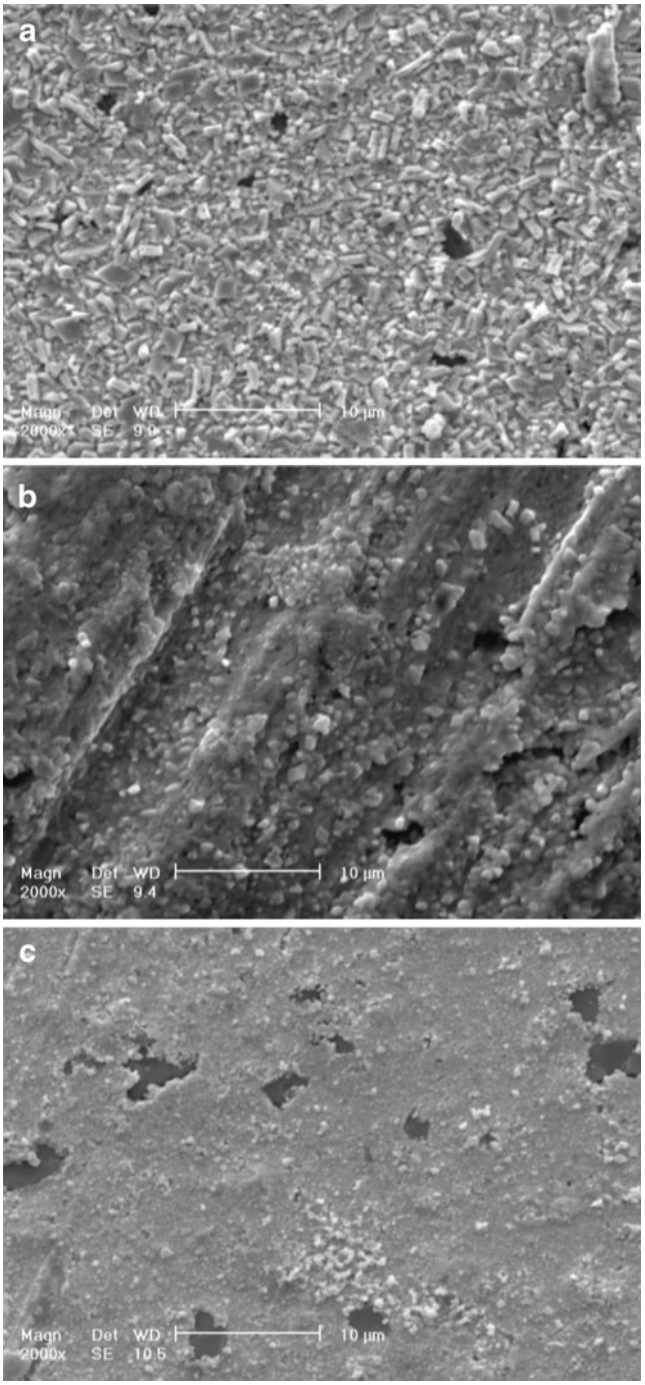

Fig. 2 The scanning electron micrographs (SEM) of Pb–1.66% Sb–Sn alloy after one cycle of charge and discharge in H_2SO_4 without additive (**a**) and in the presence of 15.0 mg cm^{-3} of IPAHS (**b**) and tri-BAHS (**c**)

Oxygen evolution overpotential

Oxygen evolution potential depends on the film characteristics because after complete conversion of $PbSO_4$ to β-PbO_2, the main reaction taking place at the electrode is oxygen gas evolution [8]. Therefore, oxygen reduction potential was investigated at the current density of 30.0 mA cm^{-2} from LSV and compared as a function of IL concentration.

Figure 4 indicates that, except BAHS that has no significant effect, other ILs have increased oxygen overpotential. Also, oxygen reduction potential slightly varies under the influence of IL concentration. The obtained results show that with increasing the number of linear alkyl chain or adding branches in alkylammonium cation, oxygen overpotential increases too. Among them, tri-BAHS is the most effective IL on the oxygen evolution potential

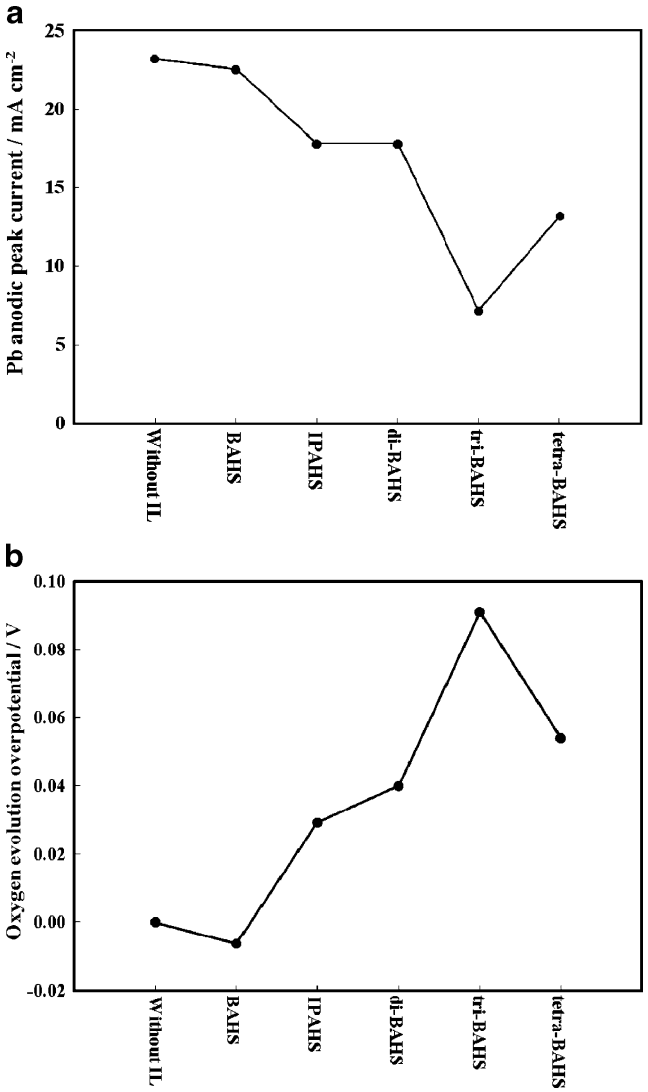

Fig. 3 Dependence of the $PbSO_4$ formation peak current (**a**) and oxygen evolution overpotential (**b**) on the number of butyl chain in ILs cation. Different ILs have equal concentration (15.0 mg cm^{-3})

(Fig. 3b). Similarity between Fig. 3a, b demonstrates that added ILs affect the morphology of $PbSO_4$, and consequently, the rate of β-PbO_2 nucleation changes and oxygen gas evolution impedes.

Hydrogen evolution overpotential

As mentioned in the previous section, hydrogen evolution potential has an undeniable effect on the performance of lead-acid battery. Therefore, it is necessary to investigate the effect of ILs on the hydrogen evolution potential.

Figure 5 shows LSV of Pb–1.66% Sb–Sn alloy for various ILs with equal concentrations (15.0 mg cm^{-3}) in 4.0 M sulfuric acid electrolyte in the region of hydrogen gas evolution. As indicated in this figure, in the presence of all three ILs, hydrogen evolution potential shifts to more

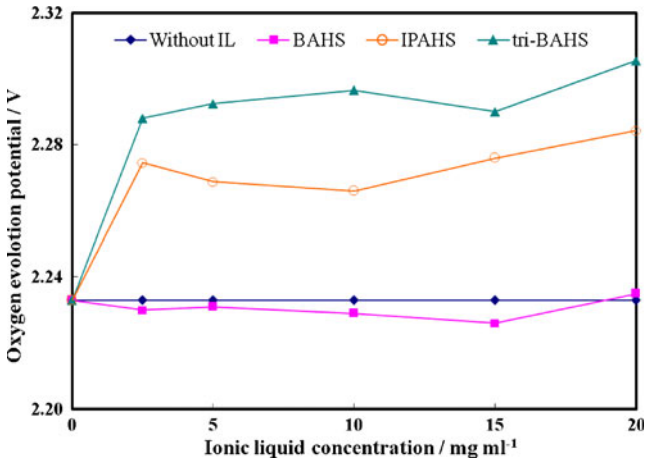

Fig. 4 Oxygen evolution potential at the current density of 30.0 mA cm^{-2} in different concentrations of ILs; working electrode: Pb–1.66% Sb–Sn; scan rate in LSV: 50.0 mV s^{-1}

negative values. Among them, tri-BAHS has the most effect on the hydrogen overpotential. Also, Fig. 6a illustrates that with increasing the number of alkyl chain in alkylammonium cation and carbon in alkyl chain, hydrogen potential has become more negative. Important point is that this increase in hydrogen overpotential has a linear correlation with the number of alkyl chain in alkylammonium cation. So, tetra-BAHS is the most effective IL, which can impede hydrogen gas evolution and, hence, water loss.

To study the effect of IL concentration on hydrogen overpotential, we recorded LSV in the region of hydrogen gas evolution in the different concentrations of IL, and then hydrogen potential was obtained at the current density of −30.0 mA cm^{-2} (Fig. 6b). It is observed that hydrogen overpotential increases with concentration of IL.

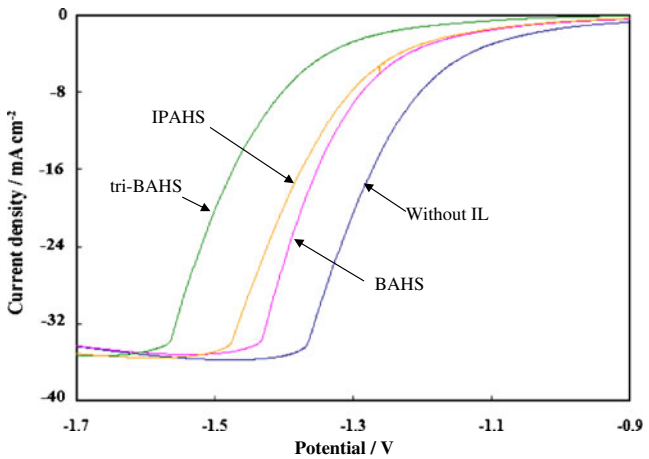

Fig. 5 Linear sweep voltammograms of Pb–1.66% Sb–Sn alloy at a scan rate of 50.0 mV s^{-1} in 4.0 M sulfuric acid electrolyte with and without ILs. The concentration of all ILs is 15.0 mg cm^{-3}

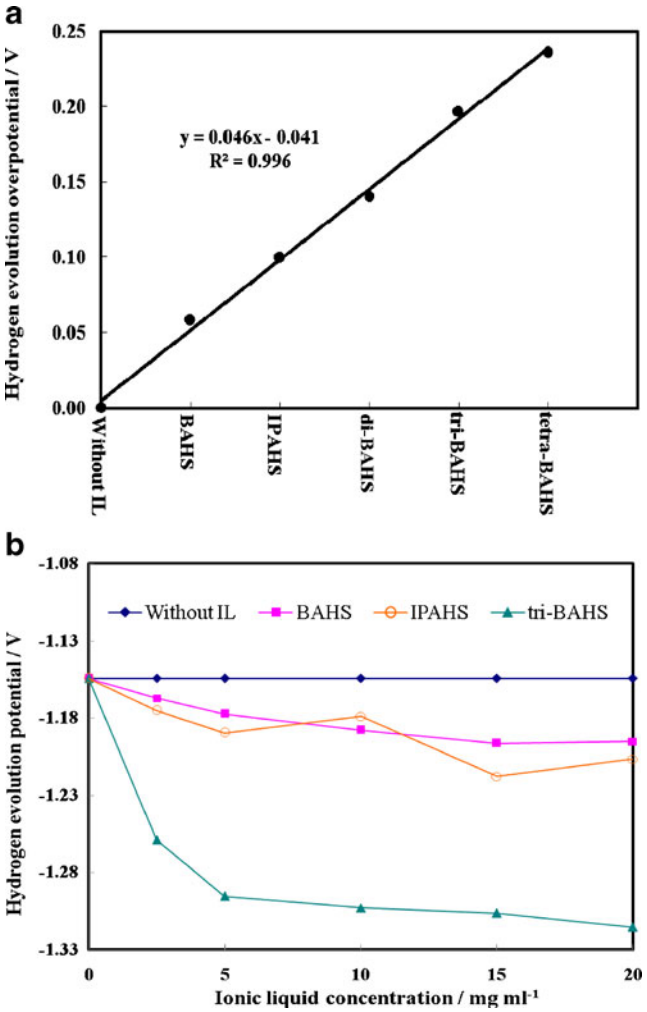

Fig. 6 Hydrogen evolution potential at the current density of -30.0 mA cm^{-2} in the presence of 15.0 mg cm^{-3} of different ILs (**a**) and in the presence of different concentration of ILs (**b**); working electrode: Pb–1.66% Sb–Sn; scan rate in LSV: 50.0 mV s^{-1}

In the previous section, it was pointed that antimony has a catalytic effect on hydrogen evolution and with increase in the Sb content of lead alloy; hydrogen evolution potential becomes more positive. Therefore, to investigate the effect of ILs on this antimony catalytic behavior, we obtained hydrogen evolution potential in the different concentrations of antimony in the working electrode. As indicated in Fig. 7, similar to acidic solution without an additive, hydrogen reduction potential has increased in the solution containing additive. It means that alkylammonium cations cannot eliminate this antimony catalytic effect.

With regard to the Nernst equation and equality of conditions (like temperature, pressure, and working electrode) in all experiments, the decrease of hydrogen ion activity is an important factor in increasing hydrogen overpotential. Indeed, the presence of alkylammonium cations in the electrolyte influences the activity of other

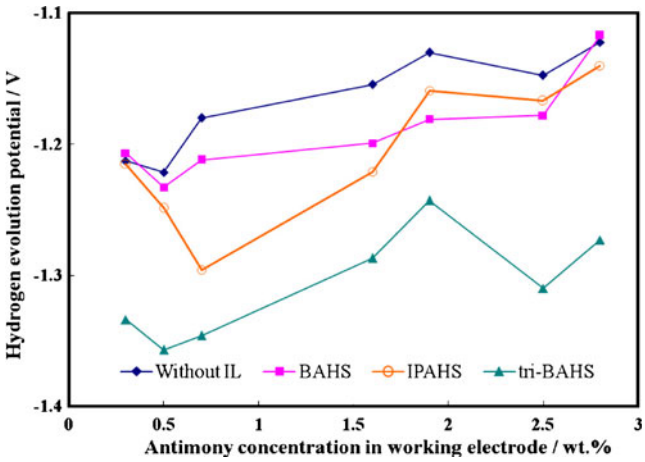

Fig. 7 Hydrogen evolution potential at the current density of -30.0 mA cm^{-2} vs. antimony concentration of working electrode in the solution containing 15.0 mg cm^{-3} of IL; scan rate in LSV: 50.0 mV s^{-1}

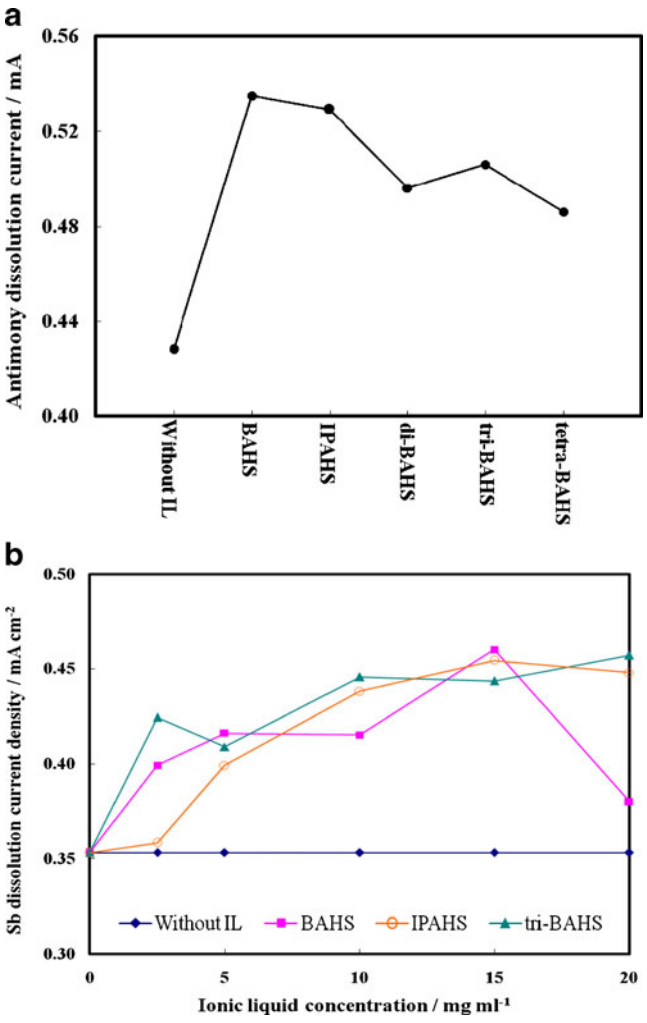

Fig. 8 Antimony dissolution current in different ILs with equal concentration: 15.0 mg cm^{-3} (**a**) and as a function of concentration of ILs (**b**); working electrode: Pb–1.66% Sb–Sn; scan rate in LSV: 50.0 mV s^{-1}

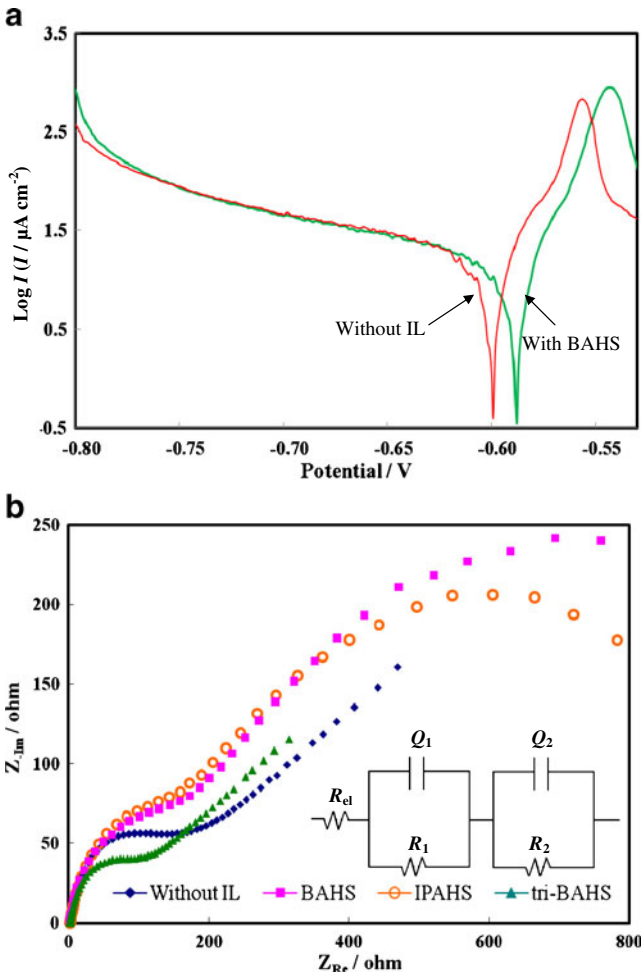

Fig. 9 Experimental potentiodynamic polarization curves in the presence and absence of BAHS (**a**); Nyquist diagrams of different ILs with equal concentration: 15.0 mg cm^{-3} (**b**); inset: proposed equivalent circuit used for fitting impedance spectra

ions and also the morphology of $PbSO_4$ layer and, thus, changes hydrogen ion concentration beneath $PbSO_4$ membrane. The result of this behavior is a noticeable effect of IL on the hydrogen ion activity and, consequently, hydrogen evolution potential.

Dissolution current of Sb

Antimony from the positive grid can migrate through the electrolyte and be deposited on the surface of the negative plate, where it lowers the overpotential for hydrogen evolution [35]. This leads to lower charge voltage, increased self discharge, and therefore, increased water loss of the battery. Therefore, antimony oxidation current (peak A_2 in Fig. 1) was used to consider antimony dissolution in electrolyte with and without ILs.

Figure 8a, b shows that Sb dissolution increases in the presence of all alkylammonium cations. However, a decreasing trend is observed with increasing the number of butyl chain. It seems that because of interaction between alkylammonium cation and other ions in the electrolyte, Sb^{3+} species become more stable, and it causes dissolution of antimony to increase. Stability of solution Sb^{3+} species is a beneficial effect because it prevents from deposition of antimony on the negative electrode, where it diminishes the overpotential of hydrogen evolution.

Grid corrosion studies

In principle, corrosion of lead starts at equilibrium potential of the negative electrode. It is important to remark that the corrosion behavior analysis of the present work differs from studies of PbO/PbO_2 formation, which consider at much higher potentials [32, 37]. At open-circuit potential, discharge reaction and hydrogen evolution have to balance each other, because no current flows through the electrode. The result of this balance is the corrosion potential (E_{corr}), in which no external current (i_{corr}) appears. In this article, the effect of the presence of ILs on the electrochemical corrosion behavior of Pb–1.66% Sb–Sn electrode in sulfuric acid solution was investigated using EIS and potentiodynamic polarization tests.

In the Tafel plots (Fig. 9a), E_{corr} and i_{corr} were obtained by extrapolation of linear parts of cathodic and anodic branches. Corrosion rate was calculated using the following equation: CR [mils per year (mpy)]=0.129 (ai_{corr}/nD),

Table 1 Corrosion data for Pb–1.6% Sb alloy in 4.0 M H_2SO_4 in the presence and absence of ILs obtained from Tafel polarization and EIS methods

	Concentration of IL (gL^{-1})	Tafel measurements				EIS measurements	
		E_{corr} (V)	I_{corr} (μAcm^{-2})	CR (mpy)	IE%	$R_1(\Omega)$	IE%
Without IL		−0.60	13.6	16	–	100	–
BAHS	5	−0.60	11.0	13	19	113	12
	15	−0.59	10.2	12	25	161	38
IPAHS	5	−0.60	9.2	11	31	139	28
	15	−0.59	8.9	10	38	140	29
tri-BAHS	5	−0.58	15.0	18	−12	96	−4
	15	−0.59	17.2	20	−25	88	−14

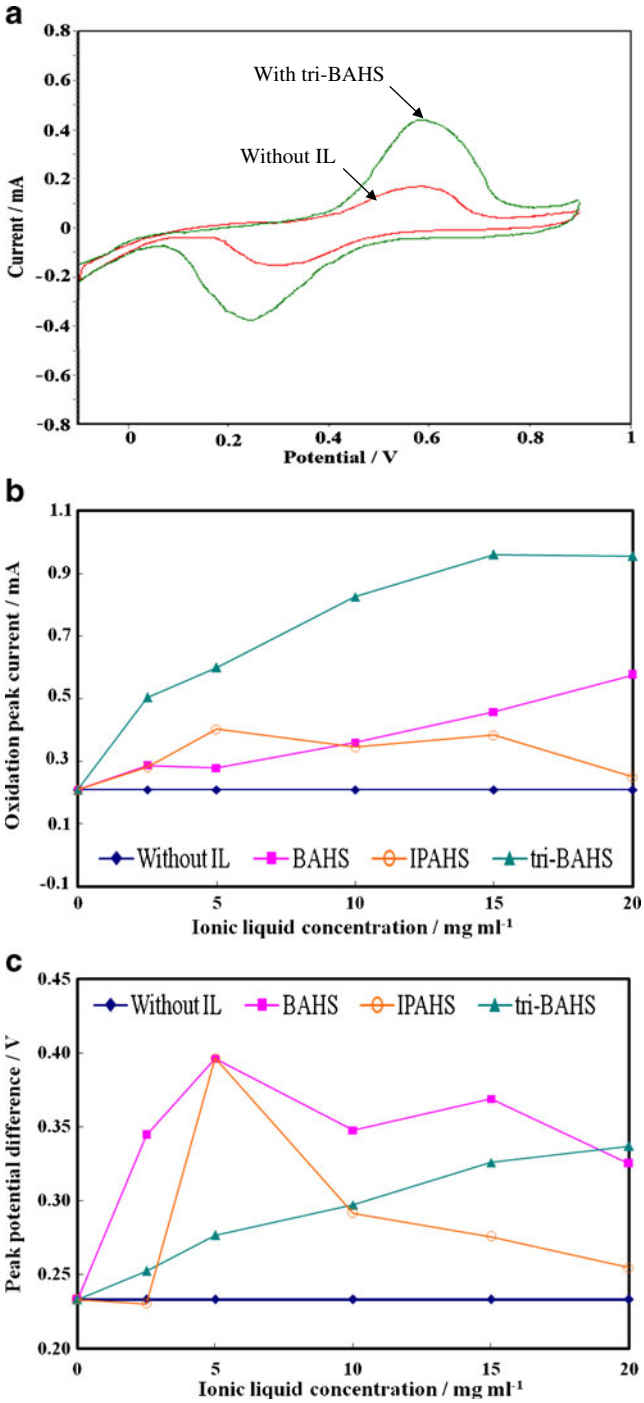

Fig. 10 Cyclic voltammograms of carbon–PbO paste electrode in 4.0 M H_2SO_4 with and without 2.5 mg cm^{-3} tri-BAHS (scan rate: 50.0 mV s^{-1}) (**a**). Oxidation peak current (**b**) and peak potential difference (**c**), according to ILs concentrations

where a is the atomic weight of alloy (g mol^{-1}), D is the density of alloy (g cm^{-3}), and n is the number of electrons that participated in corrosion reaction [38]. $IE\% = \left(1 - \left(i_{corr}/i^0_{corr}\right)\right) \times 100$. was used to calculate inhibition efficiency from polarization measurements, where icorr and ioi0corr are the corrosion current densities in the presence and absence of IL in solutions, respectively. The corrosion parameters given in Table 1 clearly indicate that the CRcorrosion rate of lead alloy decreases in the presence of BAHS and IPAHSIPAHS but increases in the solution containing tri-BAHS.

Electrochemical impedance spectroscopy is a powerful, nondestructive, and informative technique that is usually used for characterization and study of corrosion behavior. The experimental EIS results in Nyquist plots (Fig. 9b) reveal that each impedance diagram consists of two semicircles at high and low frequencies. The proposed equivalent circuit used to fit the experimental data is shown in Fig. 9b, which is similar to the one proposed in the literatures [39, 40].

It has to be noted that impedance measurements have been carried out in the open-circuit potential, where the $PbSO_4$ semipermeable membrane is formed on the elec-

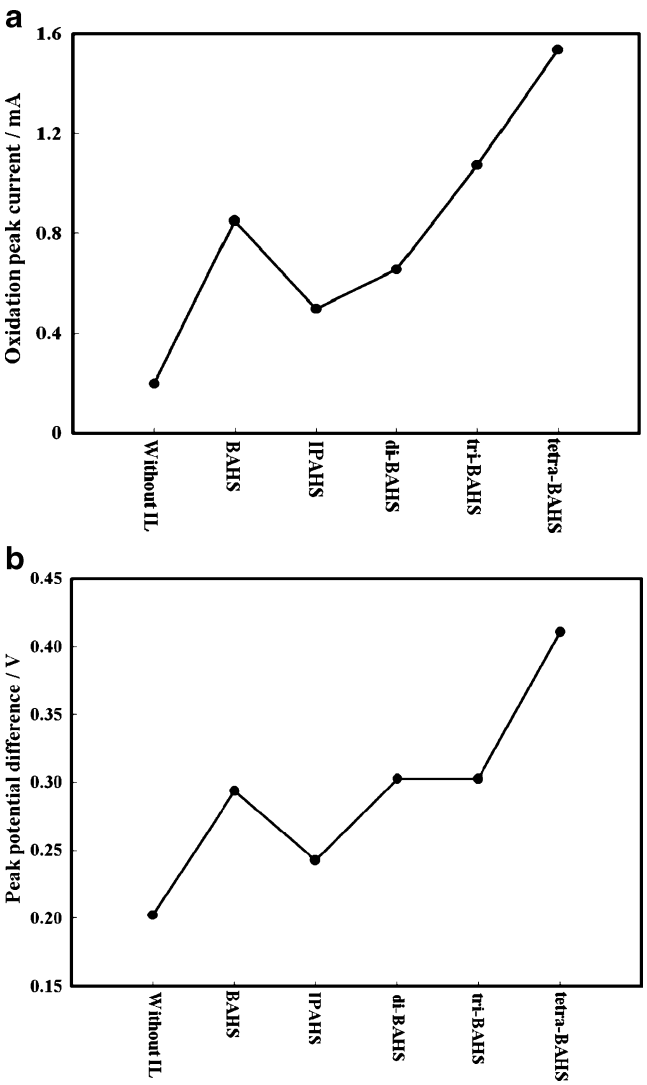

Fig. 11 Oxidation peak current (**a**) and peak potential difference (**b**) of carbon–PbO paste electrode in different ILs with equal concentration: 15.0 mg cm^{-3}

trode surface, but no PbO (stronger passivation), antimony ions, or mixed Pb–Sb oxides are formed. Therefore, in this equivalent circuit, R_{el} is the electrolyte resistance, Q_1 and R_1 correspond to the double layer capacity and the charge transfer resistance (corrosion resistance) through the vacancies of the porous layer, and the second circuit contains Q_2 and R_2, which correspond to the participation of adsorbed intermediates (all kinds of accumulated species). The impedance of a constant phase element is defined as $Q = [C(j\omega)^n]^{-1}$, where C is the capacitance, j is the current, ω is the frequency, and $-1 \leq n \leq 1$ [41, 42].

In Table 1, it can be observed that corrosion resistance (R_1) in the solutions containing BAHS and IPAHS are higher than in the solution without IL. The inhibition efficiency from impedance measurements is calculated using $IE\% = \left(1 - \left(R_1^0/R_1\right)\right) \times 100$, where R_1 and $R_1{}^0$ are the corrosion resistance in the presence and absence of IL in solutions, respectively [46]. It is in a good agreement with the results of the potentiodynamic polarization experiments. It seems that the morphological changes of the $PbSO_4$ layer, which regulate H^+ ion transport through different layers, play an important role in dictating the corrosion behavior of electrode in the presence of ILs.

Positive and negative active materials

During charge and discharge process in lead-acid batteries, Pb in negative electrode and PbO_2 in positive electrode change to Pb(II) and vice versa [36]. The electrochemical effects of ILs in conversion of $PbSO_4$ to PbO_2 and vice versa were investigated by carbon–PbO electrode. PbO in H_2SO_4 solution reacts immediately with acid, forming lead sulfate and basic lead sulfates (tribasic or tetrabasic).

As shown in Fig. 10, in the presence of different concentrations of all added ILs, conversion current of $PbSO_4$ to PbO_2 (I_a and I_c) increases, whereas reversibility, which is characterized from peak potential differences, decreases. Also, an increasing trend in I_a, I_c and irreversibility of carbon–PbO electrode were observed with increasing the number of alkyl chain in alkylammonium (Fig. 11). As it was mentioned in previous work [30], interactions between Pb^{2+} and added IL ions make more stable species of Pb^{2+}. Therefore, more $PbSO_4$ crystals are formed, which increase conversion current of $PbSO_4$ to PbO_2 that is a beneficial effect in negative and positive active materials in the battery.

Conclusion

Influence of various types of alkylammonium hydrogen sulfate, which are different in the number of alkyl chain, on the electrochemical behavior of a lead antimony electrode in sulfuric acid was investigated by using CV, SEM, and EIS methods. The results show that in the presence of all studied ILs, fewer and smaller $PbSO_4$ crystals are formed on the electrode surface. Morphological changes of the $PbSO_4$ layer play an important role in dictating the electrochemical reactions of lead alloy. All studied ILs increase hydrogen and oxygen evolution overpotential and antimony dissolution. However, they have different effects on the grid CR. Also, ILs increase the rate of the conversion of $PbSO_4$ to PbO_2, which can increase the utilization of the positive active material in lead-acid batteries.

Investigation of a family of alkylammonium hydrogen sulfate ILs shows that electrochemical behaviors of lead alloy are mainly under the influence of number of alkyl chain in alkylammonium cations. Hydrogen evolution potential has a linear correlation with the number of alkyl chain. However, oxygen evolution overpotential depends on the influence amount of IL on morphological characterizations of the lead sulfate layer. It seems that BAHSs reveal a beneficial effect on the electrochemical behavior of lead-acid battery, especially if they have a high number of alkyl chain in their cations.

Acknowledgements The authors acknowledge the Isfahan University of Technology Council and Center of Excellency in Sensor and Green Chemistry and Nanotechnology in the Environment for supporting this work.

References

1. Fogiel M (2003) Handbook of basic electricity. Research and Education Association
2. Ghasemi S, Mousavi MF, Karami H, Shamsipur M, Kazemi SH (2006) Electrochim Acta 52:1596–1602
3. Ponraj R, McAllister SD, Cheng IF, Edwards DB (2009) J Power Sources 189:1199–1203
4. Petersson I, Berghult B, Ahlberg E (1998) J Power Sources 74:68–76
5. Crompton TR (2000) Battery reference book. Reed Oxford
6. Hirasawa T, Sasaki K, Taguchi M, Kaneko H (2000) J Power Sources 85:44–48
7. Rogatchev T, Ruevski ST, Pavlov D (1976) J Appl Electrochem 6:33–36
8. Brinic S, Metkos-Hukovic M, Babic R (2005) J New Mater Electrochem Syst 8:273–282
9. Ijomah NC (1987) J Electrochem Soc 134:2960–2966
10. Bagshaw NE (1995) J Power Sources 53:25–30
11. Hameenoja E, Hampson NA (1984) J Appl Electrochem 14:449–458
12. Paleska I, Pruszkowska-Drachal R, Kotowski J, Dziudzi A, Milewski JD, Kopczyk M, Czerwinski A (2003) J Power Sources 113:308–317
13. Bhattacharya A, Basumallick IN (2003) J Power Sources 113:382–387
14. Venugopalan S (1993) J Power Sources 46:1–15
15. Ghasemi Z, Tizpar A (2006) Appl Surf Sci 252:3667–3672
16. Garche J, Doring H, Wiesener K (1991) J Power Sources 33:213–220
17. Saminathan K, Jayaprakash N, Rajeswari B, Vasudevan T (2006) J Power Sources 160:1410–1413
18. Badawy WA, El-Egamy SS (1995) J Power Sources 55:11–17

19. Voss E, Hullmeine U, Winsel A (1990) J Power Sources 30:33–40
20. Hagiwara R, Lee JS (2007) Electrochemistry 75:23–34
21. Singh PK, Kim KW, Rhee HW (2009) Synth Met 159:1538–1541
22. Ye H, Huang J, Xua JJ, Kodiweera NKAC, Jayakody JRP, Greenbaum SG (2008) J Power Sources 178:651–660
23. Sakaebe H, Matsumoto H, Tatsumi K (2007) Electrochim Acta 53:1048–1054
24. Stracke MP, Migliorini MV, Lissner E, Schrekker HS, Dupont J, Goncalves RS (2009) Appl Energy 86:1512–1516
25. Arbizzani C, Beninati S, Lazzari M, Soavi F, Mastragostino M (2007) J Power Sources 174:648–652
26. Ohno H (2005) Electrochemical aspects of ionic liquids. Wiley, New York
27. Galinski M, Lewandowski A, Stepniak I (2006) Electrochim Acta 51:5567–5580
28. Seddon KR, Stark A, Torres M (2000) J Pure Appl Chem 72:2275–2287
29. Rezaei B, Taki M (2008) J Solid State Electrochem 12:1663–1671
30. Rezaei B, Mallakpour S, Taki M (2009) J Power Sources 187:605–612
31. Babic R, Metikos–Hukovic M, Lajqy N, Brinic S (1994) J Power Sources 52:17–24
32. Pavlov D, Bojinov M, Laitinen T, Sundholm G (1991) Electrochim Acta 36:2087–2092
33. Guo Y, Wu M, Hua S (1997) J Power Sources 64:65–69
34. Sun Q, Guo Y (2000) J Electroanal Chem 493:123–129
35. Culpin B, Rand DAJ (1991) J Power Sources 36:415–438
36. Takehara Z (2000) J Power Sources 85:29–37
37. Pavlov D, Bojinov M, Laitinen T, Sundholm G (1991) Electrochim Acta 36:2081–2086
38. Fontana MG (1985) Corrosion engineering. McGraw-Hill Book Company, New York
39. Kiani MA, Mousavi MF, Ghasemi S, Shamsipur M, Kazemi SH (2008) Corros Sci 50:1035–1045
40. Popova A, Christov M (2006) Corros Sci 48:3208–3221
41. Gudic S, Radosevic J, Kliskic M (2002) Electrochim Acta 47:3009–3016
42. Osorio WR, Goulart PR, Garcia A (2008) Mater Lett 62:365–369
43. Metikos-Hukovic M, Babic R, Omanovic S (1994) J Electroanal Chem 374:199–206
44. Guo Y (1992) Electrochim Acta 37:495–499
45. Guo Y (1991) J Electrochem Soc 138:1222–1227
46. Babic-Samardzija K, Khaled KF, Hackerman N (2005) Appl Surf Sci 240:327–340